CARDIFF UNIVERSITY
PRIFYSGOL CAERDYDD

ORCA – Online Research @ Cardiff

This is an Open Access document downloaded from ORCA, Cardiff University's institutional repository:https://orca.cardiff.ac.uk/id/eprint/107824/

This is the author's version of a work that was submitted to / accepted for publication.

Citation for final published version:

Morgan, David J. 2019. Imaging XPS for industrial applications. Journal of Electron Spectroscopy and Related Phenomena 231 , pp. 109-117. 10.1016/j.elspec.2017.12.008

Publishers page: http://dx.doi.org/10.1016/j.elspec.2017.12.008

Please note:
Changes made as a result of publishing processes such as copy-editing, formatting and page numbers may not be reflected in this version. For the definitive version of this publication, please refer to the published source. You are advised to consult the publisher's version if you wish to cite this paper.

This version is being made available in accordance with publisher policies. See http://orca.cf.ac.uk/policies.html for usage policies. Copyright and moral rights for publications made available in ORCA are retained by the copyright holders.

Imaging XPS for Industrial Applications

David J. Morgan

Cardiff Catalysis Institute, School of Chemistry, Cardiff University, Park Place, Cardiff. CF10 3AT. UK

And

EPSRC National Facility for XPS (HarwellXPS), Room G.63, Research Complex at Harwell (RCaH), Rutherford Appleton Laboratory, Harwell, Oxford, Didcot, OX11 0FA. UK

E-mail: MorganDJ3@Cardiff.ac.uk

Abstract

Imaging XPS has been available on commercial XPS instruments since the 1990's, however its exploitation in the elucidation of surface chemistry has been minimal due to historical limitations in spatial resolution and acquisition times. Major developments in both instrumentation and multivariate data analysis techniques have improved greatly on all these aspects and herein a range of imaging analysis to illustrate the power of XPS imaging to a diverse range of industrial sectors is presented.

Introduction

X-ray photoelectron spectroscopy (XPS) is well established as one of the most powerful, yet easy to access surface analytical techniques [1]. However, despite major advances in spectrometer design and application, the use of imaging XPS as a technique for problem solving surface phenomena is often overlooked.

Rationally, XPS imaging is an extension to small area XPS [2, 3], whereby a map or image of the surface is produced, with X-Y coordinates revealing the elemental distribution and therefore chemical state of the samples surface. The first true commercialised foray in to XPS imaging, affording a spatially resolved X-Y image, was that by VG Scientific with their ESCASCOPE instrument [4, 5]. Here, an extra lens was placed at the analyser entrance slit to convert X-Y data into angular information and a second placed before an imaging detector which converted the data, *via* Fourier-transform, to an energy filtered X-Y image. Despite the limited count rate at the time, this was the first example of a true parallel imaging system. Perhaps the oversight in the application of imaging XPS is undoubtedly due in part to these historically long data acquisition times and also limited spatial resolution [6]. Additionally, this also means that expertise in handling and interpretation of such image data in the XPS community is generally deficient.

Such issues are actively being addressed by instrument manufacturers, with the latter also being addressed by independent software developers [7, 8].

The Basics of XPS Imaging

Typically, different instrument manufactures have a preferred way of obtaining images for XPS analysis with spatial information; these include (a) localisation of the incident x-ray probe, through micro-focussing, (b) limiting the analysis area, or, (c) application of array detectors with imaging optics.

These approaches can themselves be divided into two broad classifications, specifically i) serial imaging and ii) parallel imaging, which are considered below:

i) Serial Imaging

In serial imaging, maps of the surface are constructed by collecting the data point-by-point, with synchronous pixel-by-pixel reconstruction of the image. This can be achieved by:

a) Movement of the sample stage with the X-ray focal point fixed
b) Scanning a focused X-ray probe across the area of surface (*Probe Defined*)
c) Control of the area for electron emission (*Lens Defined)*

The first of these modes can be readily applied when imaging over relatively large areas is required (such as several square millimetres), since the stage can be rapidly moved whilst continuously collecting the emitted electrons. The second, so-called probe-defined method takes monochromated X-rays and scans the surface by rastering the electron beam used to generate the x-rays over the anode surface and thorough synchronisation of the raster area with the detection timings, an image is produced. Finally, the lens-defined mode is optimally used when relatively large areas are required. Here, the area over which the electrons are collected from is controlled by means of an area defining aperture and transfer lens. The required area is then achieved by variation of the voltages on deflector plates within the transfer lens system.

For these cases, using an array of detectors such as a channelplate detector, or a bank of channeltrons, allows the possibility for increasing the overall sensitivity of the technique through summation of neighbouring energy channels/detectors. Systems employing these methods include Thermo Scientific's Theta-Probe, K-Alpha and Nexsa series and the PHI Quantera SXM. The Thermo Scientific K-Alpha$^+$ spectrometer for example, allows imaging over small areas by changing the spot size of the X-ray probe, by means of a microfocused monochromator from 400 µm down to 30 µm (in 5 µm steps), with the latest Nexsa system allowing imaging down to 10 µm also. In such imaging modes, the microfocused beam is rastered across the sample by rapid stage movements, yielding a x20 increase in imaging speeds when compared to traditional mapping techniques and with a variable field of view (FoV) from 0.5 mm^2 up to 3 mm^2, with full spectra acquired at each pixel.

ii) Parallel Imaging

In recent years, parallel imaging has increased in popularity for the construction of elemental maps and chemical speciation of surfaces. In this mode, electrons are collected from the whole FoV without the area defining methods discussed for serial imaging.

Briefly, such imaging is achieved by the electrostatic projection of the photoelectrons within a pre-selected energy range from the sample's surface through the analyser to a 2D-detector. In such analysis, a concentric hemispherical analyser (CHA) or spherical mirror analyser (SMA) energy analyser may be used, although Kratos in their Axis range of instruments, contain both a CHA and SMA, the former used for spectroscopy and the latter for parallel imaging [9-11].

Advantages over this approach relative to the serial acquisition are improvements in spatial resolution, with values <5 µm possible and greatly improved image collection times without loss of sensitivity – a 256 x 256 pixel image can be recorded in seconds [9, 12]. Such speed increases allow for routine 'imaging stitching'; a combination of parallel imaging with automated stage movements affording the acquisition of high spatial resolution images over areas of several square millimetres.

Of notable mention here are photoemission electron microscopy (PEEM) systems, such as the NanoESCA from Omicron. Such systems yield an unparalleled lateral resolution of 650 nm (0.65 µm) in a standard laboratory environment, although the high electric field generated between the sample and the cathode lens system used, limits the use for insulating samples [13-15].

Regardless of the acquisition method, it is evident that intensity changes in an image should reflect a change in the chemical composition of the surface under study. However, care must always be taken, especially for rough surfaces, as deviations in the image contrast can be influenced by changes in the elemental or chemical composition and the topography of the surface. Such topographical changes may cause x-ray 'shadowing' which prevents or minimises photoelectron emission, therefore photoelectron intensities from such shadowed areas will be much lower; such phenomena has been discussed in detail by Artyushkova and Fulgham [16] and the interested reader is directed to their work for further information.

With XPS imaging, ultimately, the need to also look at conventional XP spectra may remain, although whether this is done at the time of image acquisition, or later by reconstruction of XPS data from the image data, is perhaps at the discretion and confidence of the analyst.

Herein, whilst some of the systems discussed are relatively simple, these have been purposely chosen to demonstrate the power and advantages in XPS image acquisition in respect of potential industrial areas of use. It is therefore hoped the realisation of the strengths of imaging XPS will allow for greater consideration and adoption in a wide range of industries.

All original data presented in this paper was acquired using a Kratos Axis Ultra DLD spectrometer or a Thermo K-Alpha$^+$ spectrometer operating in one of modes discussed.

Developments in XPS Imaging

Quantitative Spectroscopic Imaging (Spectromicroscopy)

Prior to the development of delay-line detectors, XPS imaging did not provide any quantitative information [9]. Since such developments, over the last decade or so, development of traceable and quantitative analysis methods for XPS image analysis have been reported [9, 17-19]. However, XPS spectrum image data sets acquired using standard laboratory spectrometers tend to have inherently poor signal-to-noise, and therefore require the use of multivariate analytical techniques to achieve data scaling and avoid prohibitively long acquisition times [19-24].

The vast improvements made in data acquisition allow for larger, more complex data sets to be recorded and analysed, with spectra reconstructed from such image data sets. As illustrated in figure 1, for such experiments, spectroscopic regions are defined and recorded so that they include the elements of interest and the intensity of each pixel (or more commonly a group of pixels in a given area) is plotted as a function of binding energy. This ultimately achieves small spot XPS analysis from multiple areas of an image, with the possibility of the generation of spectra from much smaller areas than is typically possible using the more common small-spot area data acquisition.

Through the generation of such spectra-at-pixel, standard spectroscopic data processing techniques can be applied for each spectrum. Problematically, the short acquisition times lead to very poor signal to noise ratios for a spectrum from a single pixel, however, the large datasets generated are suitable for multivariate analysis which can be used to gain significant improvement in signal to noise and further information on the underlying surface chemistry [7, 19, 20, 22, 24]; the examples which follow highlight such analysis.

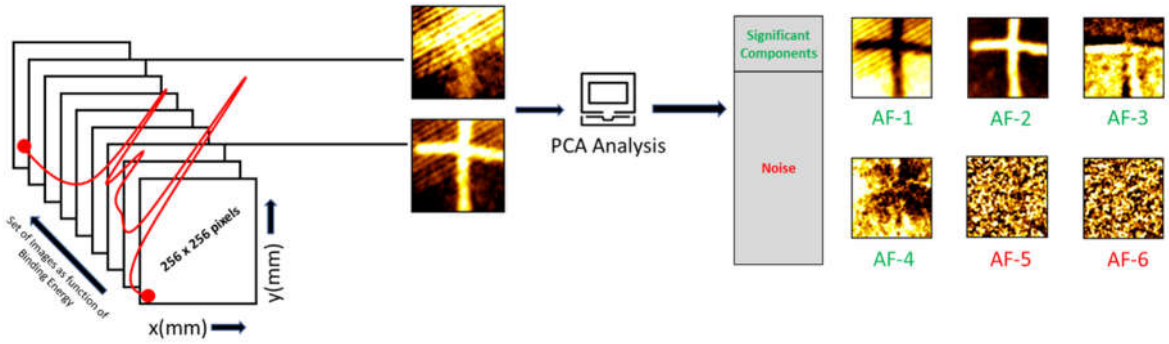

Figure 1. Schematic of obtaining spectra from images through multivariate analysis *via* principal component analysis (PCA) for noise reduction. It is possible to use the abstract factors (AF) from the image dataset to reconstruct a spectrum with enhanced signal-to-noise.

Applications of XPS Imaging

The wealth of technologies in which an understanding of the surface chemistry is paramount, is ever increasing, and the complexities of these surfaces, be it through judicial design or modification, often result in patterned surfaces well suited for imaging [25]. Whilst 20 years ago, the applicability of imaging XPS may have been limited to samples with visible and significant heterogeneity of the surface, developments made both for systems and data processing allow for the analysis and interpretation of much smaller features.

XPS imaging has therefore understandably found application in the areas of oxidation, corrosion and magnetism [26-30], surface binding and diffusion [31, 32], polymer surface chemistry [27, 33-35] and geological applications [36]. What follows are examples of different applications where imaging XPS has been successfully applied to industrially relevant situations.

1. Biological Arrays

One powerful feature of imaging XPS is the ability to perform both elemental and chemical state imaging to map the localisation of a given moiety. This may be achieved through imaging of the binding energy corresponding to a unique element or chemically distinct fragment (e.g. C-F bonds, *ca.* 290 eV), which itself is sufficiently shifted from the elemental backbone (e.g. C-C bonds, *ca.* 285 eV), of the molecule [35]. Diverse examples of such imaging can be found in the literature, which include, medical textiles [37], atmospheric particulates [38] and the lignin content of wood and its derivatives [39].

Such analysis can readily be applied to biological applications. Figure 2 shows a series of simple “peak – background” images, which have been normalised by elemental sensitivities [7], for a cross-coupling microarray used by a pharmaceutical company interested in bio-sensing applications. Briefly these systems comprise of a regular array of Au spots printed on a glass substrate, which are subsequently propagated with an organic species to facilitate reaction; examples of this type of array and analysis can be seen in ref [40], or similar analysis for DNA microarrays in ref [41].

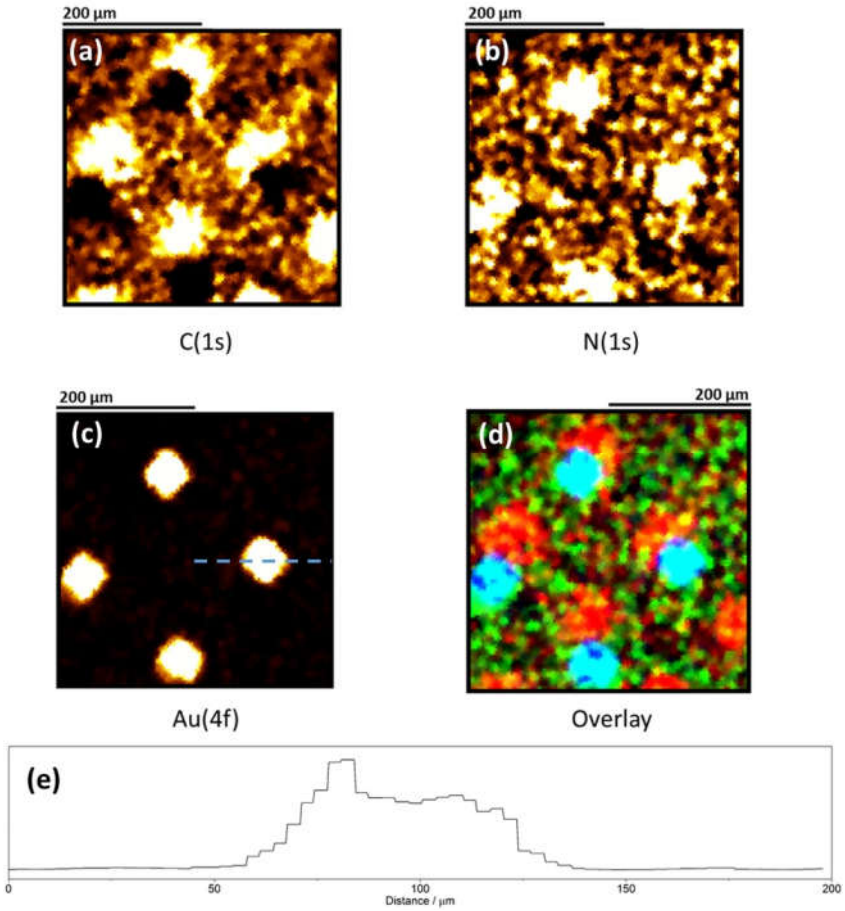

Figure 2. Peak-background XPS image spectra (FoV *ca*. 400 µm^2) for (a) C(1s), (b) N(1s) and (c) Au(4f) photoelectrons, together with (d) an overlay of all three regions, and (e) a linescan across one of the Au spots indicating its dimensions

Clear from the scaled images in figure 2, and more so in the overlay image, is the localisation of nitrogen with the Au which indicates successful anchoring to the Au and a C-C containing species around the periphery of the Au particles, which are discretely grouped, suggesting that steric effects are forcing the direction of the carbon moiety. It is worth noting, that the N(1s) signal is not from a species directly bound to the Au, but is part of a 'N(O)-C-S' containing chain. The reason for the judicial analysis of the N(1s) signal over that of sulphur was two-fold; firstly, the N(1s) signal was chemically shifted (*ca.* 405 eV) from that of other amine-like nitrogen present (*ca.* 400 eV) and secondly, the strong Si background signal precluded sufficient analysis of the sulphur and thus and allowed quick identification of the anchoring over a wider FoV than conventionally acquired spectra.

Such analysis whilst rapid, has some limitations. For example, as for conventional XP spectroscopy, the accuracy in quantification of atomic concentrations is subject to the availability of relative sensitivity factors (RSF) for the measured intensities used for the maps; therefore, any reported atomic concentrations will only be as good as the RSF's used. However, this does not detract from the qualitative nature of the images, since normalisation of each image to the total image intensity removes artefacts from the computed images.

2. *Failure Analysis and Corrosion*

One of the greatest issues industry faces is the failure of manufactured parts, which is typically caused by oxidation or corrosion [28, 42]. Imaging XPS has been successfully applied to many systems, including adhesive joint failure [43], pitting corrosion in Inconel [26], Ni-Cr-Mo alloys [44] and the analysis of contaminated channelplates [45]. In some cases, the thickness of oxide islands has been observed [7, 29].

The following example focuses on failure of a printed circuit board (PCB). Although the complexity of PCB's has changed considerably over time – for example a greater component density and more direct surface mounted components – the causes of failure are still relatively common; specifically, corrosion, broken contacts and tracks, cold-solder joints, misaligned components and surface residue contamination.

In the presented case, failures were occurring on the contact pads, where components were detaching from them; the pads themselves comprised of a conventional copper-nickel stack with a gold capping layer, approximately 0.1 µm (100 nm) thick.

Figure 3 shows selected quantified images for one of the affected PCB solder pads. The Sn of the solder is clear, but signals for Cu and Ni are clearly surprising, given the expected thickness of Au on the top of these pads.

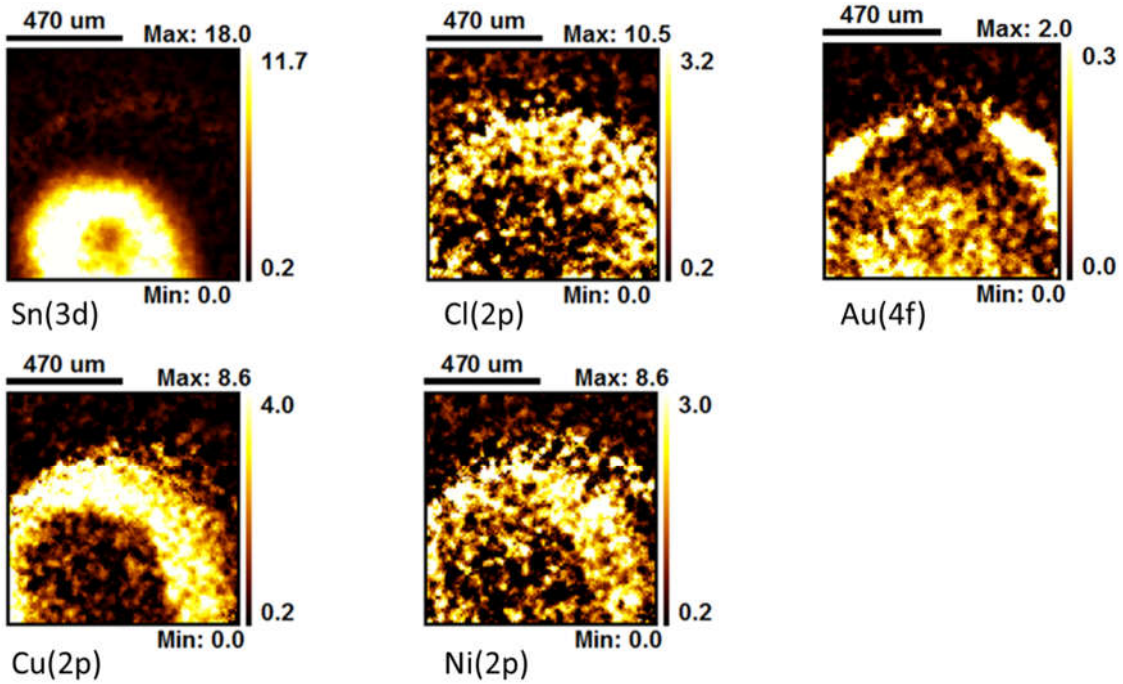

Figure 3. Quantified XPS image spectra (FoV *ca.* 900 µm^2) for the elements Sn, Cl, Au, Cu and Ni which were identified from initial 700x300 µm large area spectroscopy survey analysis.

Taken with the evidence of poor Au coverage and the presence of chlorine, it suggests a corrosive agent has etched the metallic stack. This can be confirmed by another strength of the developments in processing of XPS image data; the ability to categorise regions by a false

colour image and sum spectra according to colour classification after PCA reduction has been applied [7, 22, 46] and shown in figure 4.

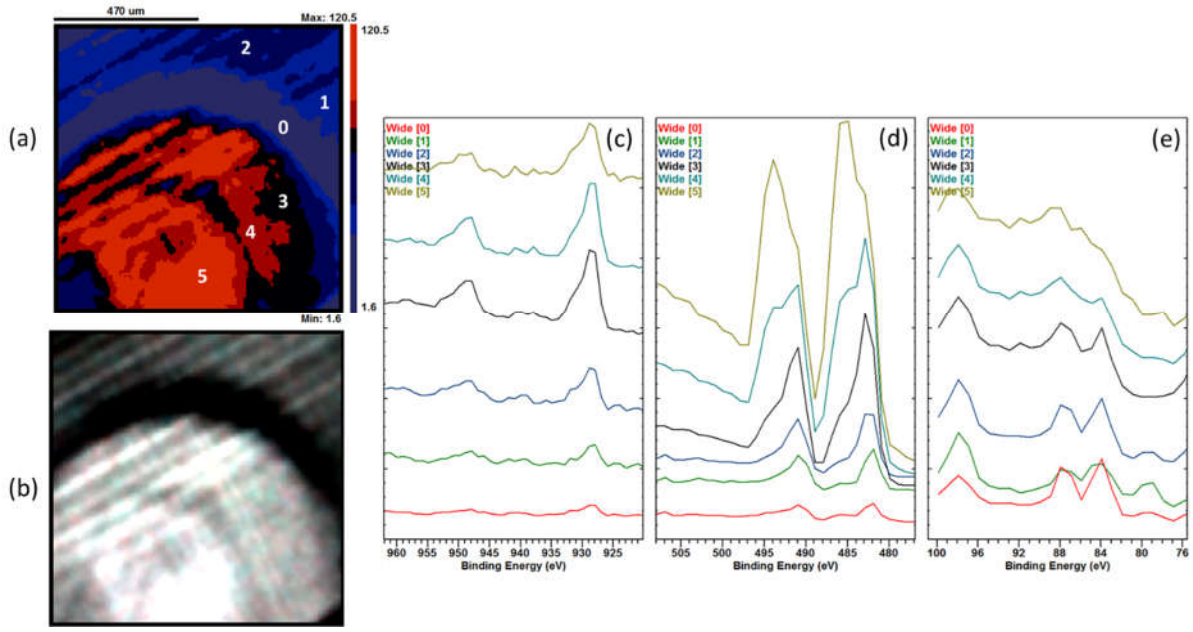

Figure 4. (a) False colour image of (b) showing one of the imaged PCB contact points and neighbouring PCB, (c) Cu(2p), (d) Sn(3d) and (e) Au(4f) reconstructed spectra from the processed image data. The numbers correspond to the different areas of interest as shown in the spectra. The observed striations in the image are due to the delay line detector.

From the reconstructed spectra shown in figure 4(c) – (e) it is evident that the underlying chemical states varying in each distinct area. Since conventional XPS analysis is an averaging technique, the points selected for analysis would reveal different chemistries (or at least an average of the surface chemical gradient) and possibly lead to an erroneous, or at best partial, conclusion for the root cause of failure. To complement any conclusions, a logical extension to the analysis of image data, such as those shown in figures 3 and 4, is the ability to partition fitted spectral data so that distinct binding energies (hence chemical states for the same element) can be readily observed [7].

As an illustration, figure 5 shows the same PCB, where the Sn(3d) image data has been partitioned into two chemical states for Sn(0) (figure 5a) and Sn(II) (figure 5b). A complete analysis would also partition differences in any of the other elemental chemical states, such as Au(0) and Au-Cl states.

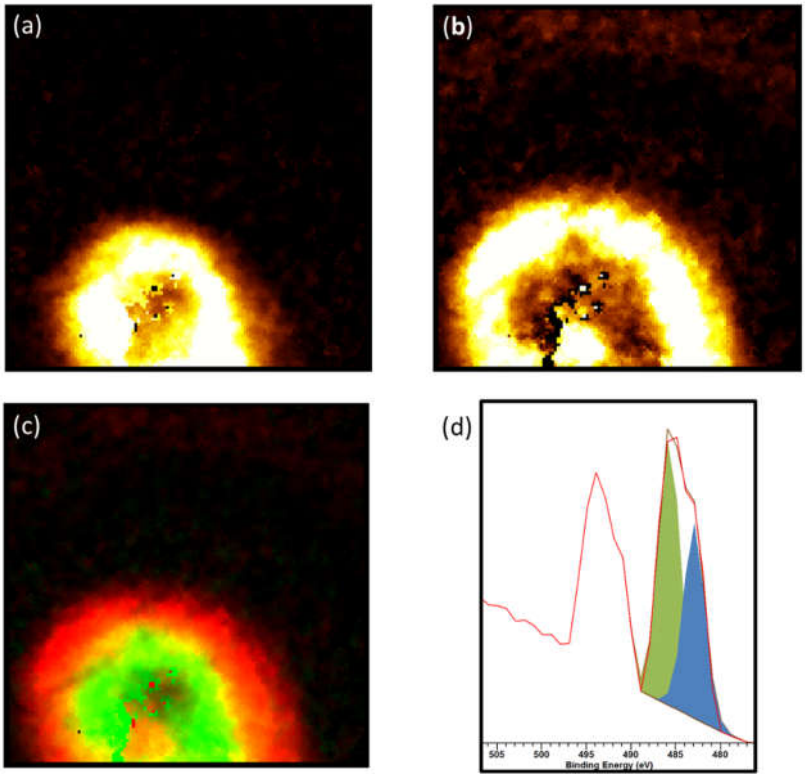

Figure 5. Sn(3d) image data for (a) Sn(0) (binding energy 485.2 eV), (b) Sn(II) (binding energy 486.6 eV), (c) overlay of the two chemical states showing some overlap between the Sn states and (d) one of the curve fits obtained from pixel spectra used to generate the chemical state images; note the spectra are uncalibrated.

As already stated, these conclusions could be obtained by several small-spot XPS analysis. However, the greater FoV afforded by imaging, together with the direct visualisation of the elements, removes the need for judicial pre-selection of analysis areas; indeed, rapid parallel imaging can facilitate the identification of areas for small-spot XPS analysis, especially over larger areas.

3. Catalysis

Industrially, the use of catalysis has been evident since the simple systems of the 18th century [47] and, as technology has improved, the evolution of catalysts in to more complex, multicomponent materials has expanded since the turn of the 20th century [48]. Since catalytic processes occur on the surface of the catalyst, an understanding of the surface chemistry, activity and behaviour of a catalyst is of immense importance, if successful transfer and scale-up from a research laboratory to an industrial environment is to be realised.

An example of a catalytic system which has undergone such transition, is the that used for acetylene hydrochlorination [49-51]. Details of the catalytic system can be found in the preceding references, but briefly, low levels of gold are dispersed on the surface of carbon extrudes giving an egg-shell type appearance as illustrated in Figure6(a). The dispersion and

speciation of the gold is critical to the activity of the catalyst and controlled preparation of the catalysts is vital in achieving this [50, 52].

Figure 6 shows the results obtained from a catalyst pellet acquired using a micro-focused x-ray probe, combined with rapid stages movements as discussed earlier. Here a carbon extrudate (seen in figure 6(b)) was taken from a catalyst batch exhibiting minimal activity and imaged. Conventional XPS spectroscopic analysis, had already revealed widely differing gold concentrations in a linescan type analysis across the extrudate, with imaging XPS employed to ascertain gold content and dispersion over a much larger area (*ca*. 3 mm^2) than spot analysis may achieve. As shown in figure 6(c) and (d), a region of high gold nucleation was found, with both Au(0) and Au(III) species; the latter whilst associated with catalytic activity *via* a Au(I)-Au(III) redox couple [51, 52], the poor dispersion is clearly the reason for the minimal activity observed.

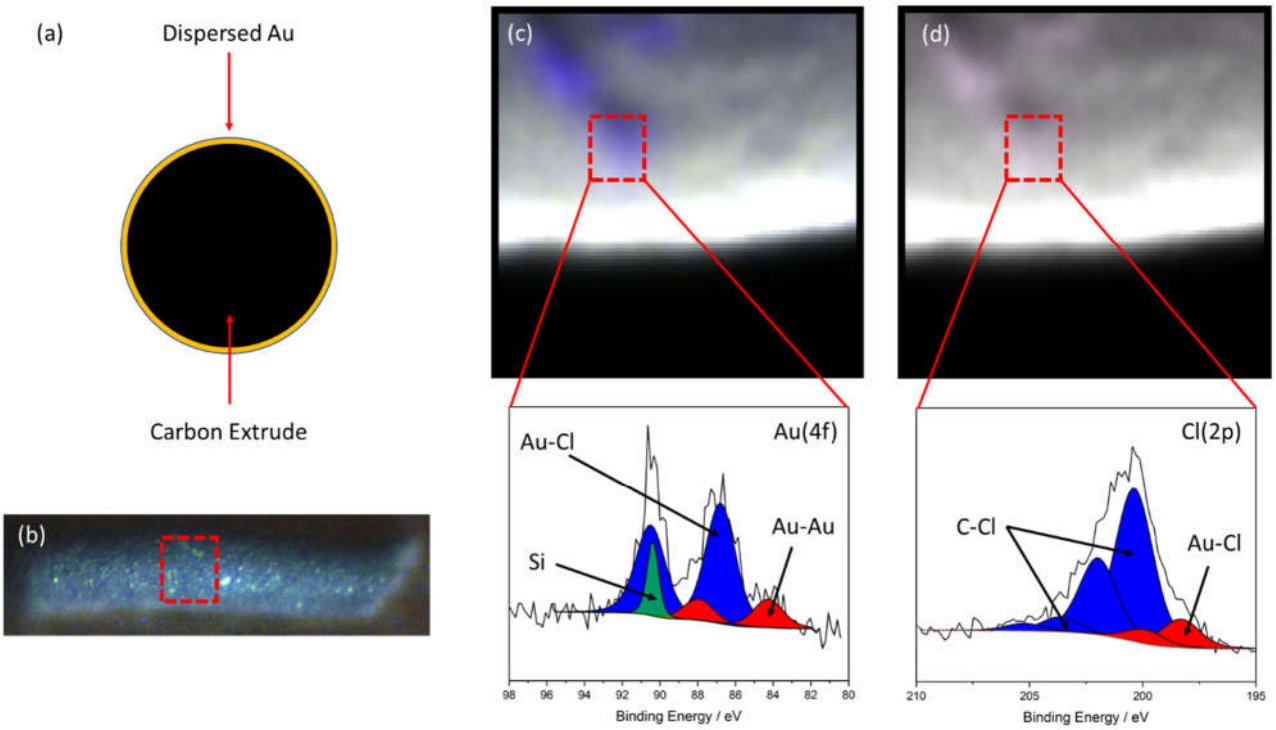

Figure 6. (a) Schematic of the egg-shell type catalyst, (b) optical image of the carbon extrude with the analysed area highlighted, (c) Au(4f) and (d) Cl(2p) processed 3x3 mm^2 'snapmap' images, with fitted core-level spectra reconstructed from pixel spectra.

It should be appreciated, that the resolution limits of modern spectrometers are a few microns and therefore too coarse to image atomic details. However, the chemical gradients in cross-sections of catalytic monoliths or differences between catalyst pellets are well within this range to make such imaging analysis viable and routine for such systems.

4. Applications to Carbon Based Technologies

Since the exfoliation of graphene was first reported in 2004, [53] graphene and related materials have has attracted a great deal of interest, with researchers exploring these materials for a range of industrial applications [54]. Depending on the application, an understanding of both the oxygen content and carbon sp^2 and sp^3 content is critical in a detailed knowledge of the systems, which is not easily obtained through the analysis of sometimes complex C(1s) core level spectra [55-57].

For analysis of carbon materials, imaging XPS has already been applied by researchers at the National Institute of Standards and Technology (NIST), where the analysis of conductive carbon within an epoxy matrix, has been studied and mapped through utilisation of differential charging of the two different components [58].

To further map such carbon variances, Barlow and co-workers derived the so-called Multivariate Auger Feature Imaging (MAFI) method for differentiating between sp^2 and sp^3 carbon, through imaging the x-ray induced C(KLL) auger feature [59, 60], which itself is derived from the work of Lascovich *et al*. [61], who derived the "D-parameter" to quantify the amount of sp^2 carbon present in a sample.

Figure 7 shows the results from Barlow's D-parameter imaging of a graphitic flake immobilised on conductive carbon tape taken from [59].

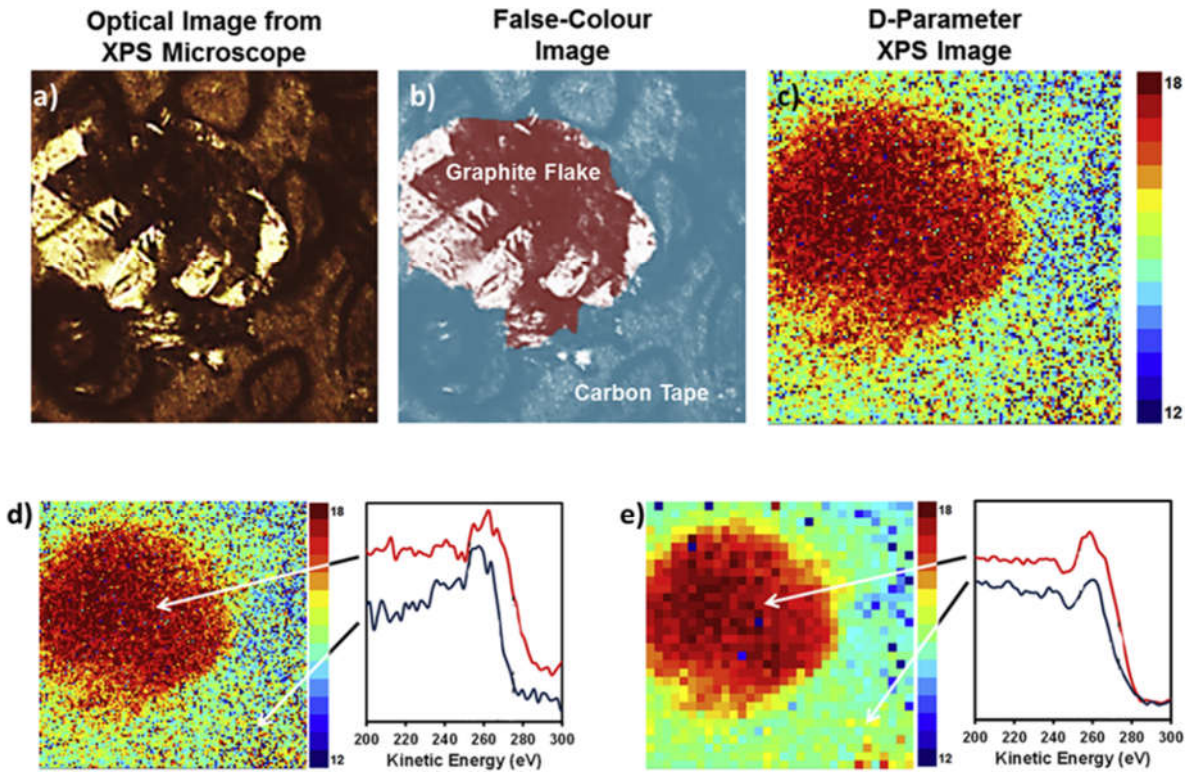

Figure 7. D-Parameter Imaging result from graphite flake mounted on carbon tape. (a) optical image from the XPS camera showing the analysis area, (b) false-colour version to differentiate the graphite flake and tape, (c) computer D-Parameter image presented as a thermal map where 'warmer' colours reflect regions of high D-Parameter (sp^2-like carbon) and 'cooler' colours indicating regions of low D-Parameter (sp^3-like carbon). Also shown are D-Parameter image with C(KLL) spectra extracted from pixel resolutions of (d) 128 × 128 and (e) 32 × 32 pixels. [Image reproduced from Ref [59] under the Creative Commons Attribution License]

Application of the MAFI technique, clearly provides strong and unambiguous identification of areas of varying sp^2 content in a rapid fashion. There is clear scope for exploitation of this technique where extended graphite/graphene networks are used, such as graphene based electronics [62].

5. Correlation with Raman Spectroscopy

Correlation with other techniques which can also capture size and homogeneity, such as those mentioned herein, can provide incredibly valuable information in a complete analysis of a surface material [59, 63]. Great developments in such correlated analysis has been made by Fulghum and co-workers, who have successfully correlated imaging XPS with AFM, FTIR and confocal microscopy [20, 33, 34, 64, 65], whilst others have sought to correlate quantitative imaging XPS with electron backscatter diffraction (ESBD) for corrosion of grain boundaries [44].

In addition to those exploited by Fulgum, correlation with Raman spectroscopy is now relatively facile with instrument manufacturers now offering XPS and Raman on a single instrument as standard, and importantly with equal probe size (ca. 10 um). Figure 8, shows the results of a combined XPS-Raman analysis for a simple system where staining was observed on a PET substrate.

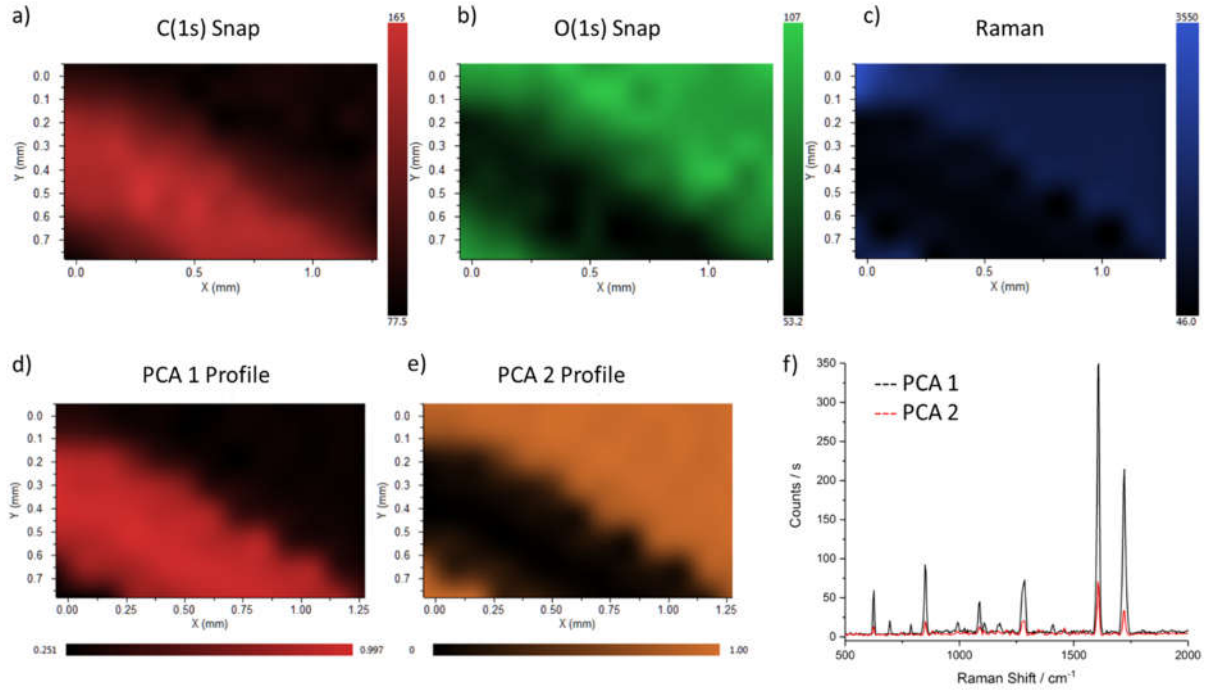

Figure 8. (a) C(1s) and (b) O(1s) 'snapmap' image spectra acquired at a 10 µm probe size, (c) corresponding Raman map acquired at 10 µm also, (d) and (e) reconstructed principle components derived from analysis of both Raman and XPS data, (f) section of the average Raman spectra from both PCA derived phases. [Data courtesy of Thermo Scientific and used with permission]

Although XPS analysis both on- and off-stain would be commonplace, the composition of the contaminant may still be elusive. However with the addition of Raman spectra and the availability of both commercial and freely available Raman spectral libraries (see for example [66]), the ability to both chemically identify and quantify each phase is more accessible and therefore opens even more avenues in industrial sectors such as pharmacy, cosmetics, geology and mineralogy.

Such analysis can be extended for the analysis of carbon materials (see section 4), where the ability to correlate for example MAFI analysis with D/G-Raman band intensities would be of high value to those involved in the manufacture of carbon material in correlating surface chemistry with graphene layer thickness and properties [67].

Comparison with Other Surface Imaging Techniques

It would be unwise not to compare imaging XPS to other analytical techniques. Many will already be familiar with other surface imaging tools, with perhaps the most commonly thought of being probe microscopies, such as AFM or STM [68-70]; although these are clearly nanoscale imaging techniques (where as imaging XPS is on the micron scale), the general lack of chemical speciation for the topographical surface features limits is usefulness without other techniques for chemical identification [68, 69]. Imaging XPS typically has a resolution of down to *ca.* 10 μm for systems employing a rastered beam, whereas parallel imaging systems can have resolutions of 1 μm under optimal conditions (typically <5 μm). Whilst these are orders of magnitude higher than that afforded by the probe microscopies, the ever-critical chemical speciation is present.

Auger electron spectroscopy (AES), ToF-SIMS, Infra-Red (IR) and Raman are all capable of imaging surfaces; see for example applications in refs [71-74]. Whilst AES has unrivalled resolution (<10 nm) with an information depth comparable to that of XPS, application to insulting systems is difficult [74]. Raman spectroscopy is essentially a bulk technique typically probing a few microns of the surface, whilst the spatial resolution of IR spectroscopy for mid-IR wavelengths is limited to somewhere between 3 and 30 μm due to diffraction limitations, although developments are being made to overcome these [75, 76]. Equally, whilst the ability of ToF-SIMS to probe the first few nanometers (*ca.* 1 – 5 nm) of a surface with <100 nm resolution is exceptional, the data is typically semi-quantitative at best.

XPS imaging, despite its resolution limitations, has great applicability to a wider range of surface analytical problems.

Conclusions and Future Directions

The applicability and strength of XPS imaging has been demonstrated using a range of samples from diverse industrial sectors.

In contrast to the conventionally held belief of imaging XPS, acquisition speeds, even for the most complex of systems, are today in line with those required for multiple small-spot spectroscopy analysis with good signal-to-noise ratio, but with potentially far greater information obtainable from PCA analysis of the image data.

The future of XPS imaging is promising, with manufacturers undoubtedly wishing and actively trying to push the boundaries of sensitivity and spatial resolution through improvements in lens and analyser design. Such development will undoubtedly be strengthened by both the current and future XPS user base wishing to maximise the available information from their samples and, as quantitative imaging and associated multivariate analysis becomes more prevalent, the application of standard XPS data analytical routines, such as curve fitting, could be routinely applied to image data.

The depth distribution of elements and nano-structure quantification from photoemission spectra is already well established [77] and recently progress has been made in the extension

of these data analysis techniques to image data [8, 78-80]; coupled with the increasing demand for analysis of nano-structures, this is likely to continue. With the development of more commonplace higher energy photon sources, such as monochromatic Ag Lα and Cr Kα, the ability to image layered structures may be possible due to the increased information depth.

Combining multiple analysis techniques, especially those capable of imaging on a single analytical system, such as XPS and Raman, will undoubtedly bring the application of imaging XPS to the forefront in many sectors. Such combinations can readily be designed so that the probe sizes of each analytical technique are coincident and of comparable size, allowing for efficient superimposition of spatially equivalent spectral and image datasets.

Acknowledgements

The author would like to thank the application scientists at Thermo Scientific, East Grinstead for supplying correlated XPS and Raman data. Some data was collected as part of the EPSRC National Facility for XPS ('HarwellXPS'), operated by Cardiff University and UCL, under contract No. PR16195.

References

[1] Surface Analysis by Auger and X-Ray Photoelectron Spectroscopy, IM Publications, Chichester, 2003.
[2] C.M. Demanet, Vacuum, 37 (1987) 465-467.
[3] K. Yates, R.H. West, Surface and Interface Analysis, 5 (1983) 217-221.
[4] E. Adem, R. Champaneria, P. Coxon, Vacuum, 41 (1990) 1695-1699.
[5] P. Coxon, J. Krizek, M. Humpherson, I.R.M. Wardell, Journal of Electron Spectroscopy and Related Phenomena, 52 (1990) 821-836.
[6] M.P. Seah, G.C. Smith, Surface and Interface Analysis, 11 (1988) 69-79.
[7] J. Walton, N. Fairley, The Casa Cookbook Part 2: XPS Image Processing, Acolyte Science, Cheshire, 2011.
[8] S. Hajati, S. Tougaard, Analytical and bioanalytical chemistry, 396 (2010) 2741-2755.
[9] U. Vohrer, C. Blomfield, S. Page, A. Roberts, Applied Surface Science, 252 (2005) 61-65.
[10] I.W. Drummond, F.J. Street, L.P. Ogden, D.J. Surman, Scanning, 13 (1991) 149-163.
[11] C.J. Blomfield, Journal of Electron Spectroscopy and Related Phenomena, 143 (2005) 241-249.
[12] N.M. Forsyth, P. Coxon, Surface and Interface Analysis, 21 (1994) 430-434.
[13] O. Renault, Surface and Interface Analysis, 42 (2010) 816-825.
[14] O. Renault, N. Barrett, A. Bailly, L.F. Zagonel, D. Mariolle, J.C. Cezar, N.B. Brookes, K. Winkler, B. Krömker, D. Funnemann, Surface Science, 601 (2007) 4727-4732.
[15] M. Escher, N. Weber, M. Merkel, B. Krömker, D. Funnemann, S. Schmidt, F. Reinert, F. Forster, S. Hüfner, P. Bernhard, C. Ziethen, H.J. Elmers, G. Schönhense, Journal of Electron Spectroscopy and Related Phenomena, 144-147 (2005) 1179-1182.
[16] K. Artyushkova, J.E. Fulghum, Surface and Interface Analysis, 36 (2004) 1304-1313.
[17] J. Walton, N. Fairley, Surface and Interface Analysis, 38 (2006) 1230-1235.
[18] J. Walton, N. Fairley, Surface and Interface Analysis, 38 (2006) 388-391.
[19] J. Walton, N. Fairley, Surface and Interface Analysis, 41 (2009) 114-118.
[20] K. Artyushkova, J.E. Fulghum, Surface and Interface Analysis, 33 (2002) 185-195.

[21] S. Béchu, M. Richard-Plouet, V. Fernandez, J. Walton, N. Fairley, Surface and Interface Analysis, 48 (2016) 301-309.
[22] J. Walton, N. Fairley, Surface and Interface Analysis, 40 (2008) 478-481.
[23] H. Piao, L. Le Tarte, W.A. Hennessy, N. Fairley, Surface and Interface Analysis, 39 (2007) 493-500.
[24] J. Walton, N. Fairley, Journal of Electron Spectroscopy and Related Phenomena, 148 (2005) 29-40.
[25] G.A. Somorjai, L. Yimin, Introduction to Surface Chemistry and Catalysis, 2nd Edition, 2nd ed., WIley, New Jersey, 2010.
[26] B.A. Kobe, S. Ramamurthy, M.C. Biesinger, N.S. McIntyre, A.M. Brennenstühl, Surface and Interface Analysis, 37 (2005) 478-494.
[27] N.S. McIntyre, R.D. Davidson, G. Kim, J.T. Francis, Vacuum, 69 (2002) 63-71.
[28] D. Rodriguez, A. Merwin, Z. Karmiol, D. Chidambaram, Applied Surface Science, 404 (2017) 443-451.
[29] E.F. Smith, D. Briggs, N. Fairley, Surface and Interface Analysis, 38 (2006) 69-75.
[30] T. Kachel, K. Holldack, W. Guda, M. Neuber, C. Wilde, Le Journal de Physique IV, 04 (1994) C9-439-C439-444.
[31] J.W. Kim, B. Son, H. Yu, H.M. Park, Y.-S. Lee, Surface and Interface Analysis, 46 (2014) 193-196.
[32] A.V. Shchukarev, R. Mattsson, L. Ödberg, Colloids and Surfaces A: Physicochemical and Engineering Aspects, 219 (2003) 35-43.
[33] K. Artyushkova, B. Wall, J. Koenig, J.E. Fulghum, Applied Spectroscopy, 54 (2000) 1549-1558.
[34] K. Artyushkova, B. Wall, J. Koenig, J.E. Fulghum, Journal of Vacuum Science & Technology A: Vacuum, Surfaces, and Films, 19 (2001) 2791.
[35] T.A. Zupp, J.E. Fulghum, D.J. Surman, Surface and Interface Analysis, 21 (1994) 79-86.
[36] G.C. Allen, J.R. Easterman, K.R. Hallam, G.J. Graveling, K.V. Ragnarsdottir, D.R. Skuse, Clay Minerals, 34 (1999) 51-51.
[37] A.J. Pauk, F. Bretagnol, G. Buyle, C. Colin, O. Lefranc, H. Rauscher, Evaluation of Plasma-Depositied Anti-Adhesive and Anti-Bacterial Coatings on Medical Textiles, in: S.C. Anand, J.F. Kennedy, M. Miraftab, S. Rajendran (Eds.) Medical and Healthcare Textiles, Woodhead Publishing Ltd, Cambridge, 2010, pp. 48-54.
[38] B.M. Hutton, D.E. Williams, Analytical Communications, 36 (1999) 17-18.
[39] A. Shchukarev, B. Sundberg, E. Mellerowicz, P. Persson, Surface and Interface Analysis, 34 (2002) 284-288.
[40] R. Schlapak, J. Danzberger, D. Armitage, D. Morgan, A. Ebner, P. Hinterdorfer, P. Pollheimer, H.J. Gruber, F. Schaffler, S. Howorka, Small, 8 (2012) 89-97.
[41] C.Y. Lee, G.M. Harbers, D.W. Grainger, L.J. Gamble, D.G. Castner, Journal of the American Chemical Society, 129 (2007) 9429-9438.
[42] E. Diler, B. Lescop, S. Rioual, G. Nguyen Vien, D. Thierry, B. Rouvellou, Corrosion Science, 79 (2014) 83-88.
[43] S.J. Davis, J.F. Watts, Journal of Materials Chemistry, 6 (1996) 479.
[44] B. Kobe, M. Badley, J.D. Henderson, S. Anderson, M.C. Biesinger, D. Shoesmith, Surface and Interface Analysis, 49 (2017) 1345-1350.
[45] J. Walton, Surface and Interface Analysis, 39 (2007) 337-342.
[46] H. Piao, N. Fairley, J. Walton, Surface and Interface Analysis, 45 (2013) 1742-1750.
[47] E.M. Jones, Industrial & Engineering Chemistry, 42 (1950) 2208-2210.
[48] J. Hagen, Industrial Catalysis: A Practical Approach, 3rd Edition, WIley-VCH, Weinheim, Germany, 2015.
[49] P. Johnston, N. Carthey, G.J. Hutchings, Journal of the American Chemical Society, 137 (2015) 14548-14557.
[50] X. Liu, M. Conte, D. Elias, L. Lu, D.J. Morgan, S.J. Freakley, P. Johnston, C.J. Kiely, G.J. Hutchings, Catal. Sci. Technol., 6 (2016) 5144-5153.

[51] G. Malta, S.A. Kondrat, S.J. Freakley, C.J. Davies, L. Lu, S. Dawson, A. Thetford, E.K. Gibson, D.J. Morgan, W. Jones, P.P. Wells, P. Johnston, C.R. Catlow, C.J. Kiely, G.J. Hutchings, Science, 355 (2017) 1399-1403.
[52] M. Conte, A.F. Carley, G.J. Hutchings, Catalysis Letters, 124 (2008) 165-167.
[53] K.S. Novoselov, A.K. Geim, S.V. Morozov, D. Jiang, Y. Zhang, S.V. Dubonos, I.V. Grigorieva, A.A. Firsov, Science, 306 (2004) 666-669.
[54] K.S. Novoselov, V.I. Fal'ko, L. Colombo, P.R. Gellert, M.G. Schwab, K. Kim, Nature, 490 (2012) 192-200.
[55] J. Díaz, G. Paolicelli, S. Ferrer, F. Comin, Physical Review B, 54 (1996) 8064-8069.
[56] A.C. Ferrari, J. Robertson, Physical Review B, 61 (2000) 14095-14107.
[57] D. Yang, A. Velamakanni, G. Bozoklu, S. Park, M. Stoller, R.D. Piner, S. Stankovich, I. Jung, D.A. Field, C.A. Ventrice, R.S. Ruoff, Carbon, 47 (2009) 145-152.
[58] J.M. Gorham, W.A. Osborn, J.W. Woodcock, K.C. Scott, J.M. Heddleston, A.R. Walker, J.W. Gilman, Carbon, 96 (2016) 1208-1216.
[59] A.J. Barlow, S. Popescu, K. Artyushkova, O. Scott, N. Sano, J. Hedley, P.J. Cumpson, Carbon, 107 (2016) 190-197.
[60] A.J. Barlow, O. Scott, N. Sano, P.J. Cumpson, Surface and Interface Analysis, 47 (2015) 173-175.
[61] J.C. Lascovich, R. Giorgi, S. Scaglione, Applied Surface Science, 47 (1991) 17-21.
[62] S. Wang, P.K. Ang, Z. Wang, A.L. Tang, J.T. Thong, K.P. Loh, Nano letters, 10 (2010) 92-98.
[63] T. Nunney, P. Mack, O. Greenwood, R. White, M. Wall, B. Strohmeier, S. Coulson, D. Evans, Microscopy and Microanalysis, 17 (2011) 1216-1217.
[64] K. Artyushkova, J.O. Farrar, J.E. Fulghum, Surface and Interface Analysis, 41 (2009) 119-126.
[65] K. Artyushkova, J. Fenton, J. Farrar, J. Fulghum, Multitechnique Fusion of Imaging Data for Heterogeneous Materials, in: Y. Zheng (Ed.) Image Fusion and Its Applications, InTech, United Kingdom, 2011.
[66] N. Buzgar, A.I. Apopei, A. Buzatu, (2009) - Romanian Database of Raman Spectroscopy (http://rdrs.uaic.ro).
[67] A. Kaniyoor, S. Ramaprabhu, AIP Advances, 2 (2012) 032183.
[68] R. Burgess, C. Buono, P.R. Davies, R.J. Davies, T. Legge, A. Lai, R. Lewis, D.J. Morgan, N. Robinson, D.J. Willock, Journal of Catalysis, 323 (2015) 10-18.
[69] J. Bushell, A.F. Carley, M. Coughlin, P.R. Davies, D. Edwards, D.J. Morgan, M. Parsons, J Phys Chem B, 109 (2005) 9556-9566.
[70] Z. Wang, C. Zhou, C. Wang, L. Wan, X. Fang, C. Bai, Ultramicroscopy, 97 (2003) 73-79.
[71] C. Hambrock, K. Vincze-Minya, S. Hild, A.W. Hassel, physica status solidi (a), 211 (2014) 1429-1438.
[72] E.J. Lanni, R.N. Masyuko, C.M. Driscoll, S.J. Dunham, J.D. Shrout, P.W. Bohn, J.V. Sweedler, Anal Chem, 86 (2014) 10885-10891.
[73] K.-I. Morigaki, A. Ohta, Journal of Power Sources, 76 (1998) 159-166.
[74] J. Wolstenholme, Auger Electron Spectroscopy, Momentum Press, New York, 2015.
[75] C. Mayet, A. Dazzi, R. Prazeres, J.M. Ortega, D. Jaillard, The Analyst, 135 (2010) 2540-2545.
[76] F. Huth, A. Govyadinov, S. Amarie, W. Nuansing, F. Keilmann, R. Hillenbrand, Nano letters, 12 (2012) 3973-3978.
[77] S. Tougaard, Quantification of Nano-structures by Electron Spectroscopy, in: D. Briggs, J.T. Grant (Eds.) Surface Analysis by Auger and X-Ray Photoelectron Spectroscopy, IM Publications, Chichester, 2003.
[78] K. Artyushkova, Journal of Electron Spectroscopy and Related Phenomena, 178-179 (2010) 292-302.
[79] S. Hajati, S. Coultas, C. Blomfield, S. Tougaard, Surface Science, 600 (2006) 3015-3021.
[80] S. Hajati, J. Walton, S. Tougaard, Microscopy and microanalysis : the official journal of Microscopy Society of America, Microbeam Analysis Society, Microscopical Society of Canada, 19 (2013) 751-760.